# Preparation of Zr-doped CaTiO₃ with enhanced charge separation efficiency and photocatalytic activity

Xiao-jun HUANG[1], Xin YAN[1], Hai-yan WU[1], Ying FANG[1], Ya-hong MIN[1],
Wen-sheng LI[1], Shuang-yin WANG[1,2], Zhen-jun WU[1]

1. College of Chemistry and Chemical Engineering, Hunan University, Changsha 410082, China;
2. State Key Laboratory of Chem/Bio-Sensing and Chemometrics, Hunan University, Changsha 410082, China

**Abstract:** A series of Zr-doped CaTiO₃ powders were prepared with the mild co-precipitation method and calcined at 850 °C for 3 h. The as-prepared Zr-doped CaTiO₃ samples were characterized by scanning electron microscopy (SEM), X-ray diffraction (XRD), UV−Vis diffuse reflectance spectra (DRS) and X-ray photoelectron spectra (XPS). XRD result revealed the presence of single perovskite phase of CaTiO₃. UV−Vis diffusive reflection spectra of Zr-doped CaTiO₃ indicated that the absorbance obviously increased in the visible light irradiation. XPS analysis showed that two types of oxygen existed on the photocatalyst surface, including lattice oxygen and absorbed oxygen. Their photocatalytic activity in the case of the degradation of methyl orange in water and photoelectrochemical activity were also tested. The 5%Zr-doped (mole fraction) CaTiO₃ sample showed the highest photocatalytic activity. The enhanced photocatalytic activity was ascribed to the change of the lattice structure, existence of oxygen vacancies and increase of the photogenerated charge separation efficiency.
**Key words:** CaTiO₃; Zr; doping; co-precipitation; photocatalysis; photoelectrochemistry

## 1 Introduction

Due to its potential applications to many environmental pollution problems, photocatalytic degradation of organic pollutants in wastewater over semiconductor has attracted much attention [1,2]. It is well known that, when a semiconductor absorbs a photon with energy equal to or higher than the band gap energy, a free electron will be excited to the empty conduction band, leaving a positive hole in the valence band. The photoexcited electron−hole pairs can be used for the degradation of organic pollutants. The holes can react with water ($H_2O$) or hydroxyl groups ($OH^-$) absorbed on the surface to generate hydroxyl radicals ($OH\cdot^-$), and the electrons may be trapped by the dissolved oxygen species to form superoxide anion radicals ($O_2\cdot^-$). These active radicals are powerful and indiscriminate oxidants for mineralizing in a wide range of organic pollutant [3]. The photocatalytic efficiency strongly depends on the

photoinduced electron−hole recombination rate and solar energy utilization [4]. It is generally considered that the recombination of photogenerated electrons and holes is one of the most detrimental factors on the photocatalytic activity [5,6].

Perovskite-type catalysts ($ABO_3$) have attracted great interest for the unique structural features, such as variety of structural phase transitions and the variable composition [7−9]. The cations at both A and B sites can be substituted by a foreign one without destroying the matrix structure, which allows controlled alternation of the oxidation state of cations or the creation of oxygen vacancies [10−14].

CaTiO₃ has a large band gap value (~3.5 eV) [15] and thus the material is not useful in the solar spectrum for photocatalytic degradation. Nevertheless, due to its unique properties, CaTiO₃ is considered as a good host material to modify the microstructure and to enhance the photocatalytic efficiency [16−19]. Titanium and zirconium belong to the IV B group and have the similar

atom radius (Ti: 2 Å; Zr: 2.16 Å) and the same valence state (+4). Therefore, it is possible for Zr atom to be incorporated into the $CaTiO_3$ lattice by substitution for Ti atom. Many researchers have demonstrated that incorporating $Zr^{4+}$ into $TiO_2$ leads to higher photocatalytic activity than that of pure $TiO_2$ [20−22], because substituted $Zr^{4+}$ for $Ti^{4+}$ might create some structural defects, which could suppress the recombination of electrons and positive holes by their trapping [23]. What's more, $Zr^{4+}$ exhibits preferential electron trapping ability related to $Ti^{4+}$ [24]. In those researches, $Zr^{4+}$ was mainly doped in the surface layer of $TiO_2$, the higher surface acidity and the creation of surface defects were proposed as the possible reason for the enhanced photocatalytic performance.

In this work, we systematically reported Zr substitution at site B in $CaTiO_3$ and studied its effect on the photocatalytic properties of obtained $CaTi_{1-x}Zr_xO_3$. The photocatalytic activities of the Zr-doped $CaTiO_3$ catalysts were evaluated by degrading methyl orange under the irradiation of simulated solar light. The influence of Zr concentration on the photocatalytic performance was investigated.

# 2 Experimental

## 2.1 Materials preparation

All reagents used in this work were of analytical grade and used without further purification. Distilled water was used in all experiments. $CaTi_{1-x}Zr_xO_3$ samples (x=0, 0.02, 0.05, 0.08) were synthesized by the coprecipitation method described as follows. Firstly, 0.5 mL ritonx-100 was dissolved into 200 mL distilled water to form solution A. Secondly, 0.05 mol of tetra-$n$-butyl titanate, calcium nitrate and zirconium oxychloride were dissolved into 100 mL ethanol in the stoichiometric proportions corresponding to different values of x in the final oxides. This mixture was defined as solution B. Solution C was formed by dissolving excessive amount of ammonium oxalate into 100 mL distilled water. Thirdly, solutions B and C were simultaneously added into solution A drop by drop. This process was carried out at ambient temperature for 4 h to make the metal ions precipitate completely. The final precipitates were filtrated, washed with distilled water and dried. After being calcinated at 850 °C for 3 h, the catalyst powder was obtained.

To investigate the photoelectrochemical performance of the samples, the electrodes were prepared as follows: 5 mg sample and 3 mg polyethylene glycol 6000 (PEG-6000) were suspended in 3 mL ethanol to produce a slurry, and then dip-coated onto an ITO (indium tin oxide) glass substrate (3 cm × 2 cm) with a sheet resistance of 15 Ω. After being dried, the as-prepared electrodes were calcinated at 400 °C for 0.5 h to remove the PEG−6000.

## 2.2 Characterization of samples

XRD patterns were acquired on an X-ray diffractometer with Cu K$_\alpha$ radiation (XRD, Rigaku D/Max 2500). Diffusion reflection spectra (DRS) collection was carried out on a Cary 100 UV−Vis spectrophotometer with an integrating sphere using $BaSO_4$ as the reference sample. X-ray photoelectric spectroscopy (XPS) measurements were carried out with a K$_\alpha$ 1063 spectrometer by using a monochromated Al K$_\alpha$ X-ray source. The morphology of the samples was detected by scanning electron microscopy (SEM, Hitachi S4800) and transmission electron microscopy (TEM, FEI Tecnai 20). The photoelectrochemical experiment was carried out on an electrochemical system (CHI−D66H, China).

## 2.3 Photoelectrochemical measurements

Photoelectrochemical tests were carried out in a conventional three-electrode single-compartment quartz cell filled with 0.5 mol/L $Na_2SO_4$ electrolyte, using a potentiostat. The ITO/$CaTi_{1-x}Zr_xO_3$ electrode was served as the working electrode, the counter and reference electrodes were a platinum black and a saturated calomel electrode (SCE), respectively. A 500 W xenon arc lamp with a photon flux of 100 mW/cm$^2$ (CHF−XQ−500W, Beijing Changtuo Co., Ltd.) with a bias of 0 V (vs SCE) was used as the excitation light source.

## 2.4 Photocatalytic experiments

The photocatalytic activities were evaluated by the degradation of methyl orange under a 500 W xenon lamp. An aqueous solution of methyl orange (50 mL, 10 mg/L) was placed in a quartz beaker and 15 mg photocatalyst was added. Prior to irradiation, the suspensions were ultrasonicated for 10 min and magnetically stirred in the dark for 30 min to reach the absorption−desorption equilibrium. In order to distinguish the performance of different catalysts, we shortened the illumination time to make sure that the methyl orange could not be degraded totally. After reaction for 30 min, 0.5 mL of the aliquots were sampled and analyzed by recording variations in the absorption band (465 nm) in the UV−Vis spectra of methyl orange using a Cary 300 spectrophotometer.

# 3 Results and discussion

Figure 1 shows SEM images of the $CaTi_{1-x}Zr_xO_3$ samples (0≤x≤0.08) at an annealing temperature of 850 °C for 3 h. The morphology of Zr-doped $CaTiO_3$ had no changes when compared with pure $CaTiO_3$. The particle size decreased with increasing the doping
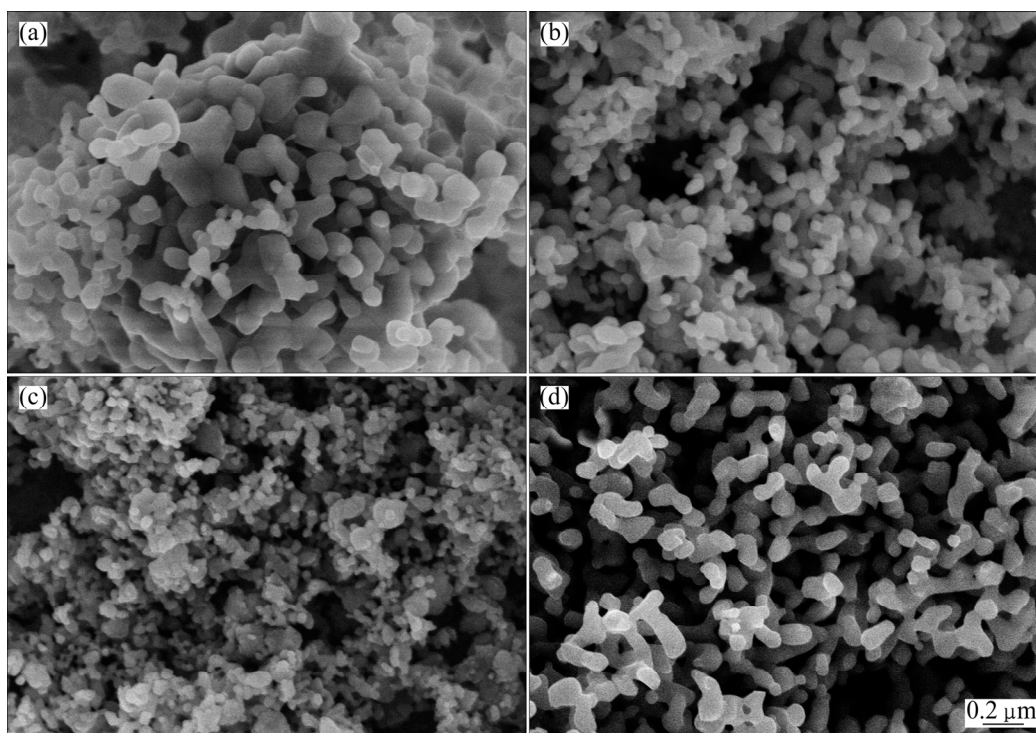
**Fig. 1** SEM images of sintered $CaTi_{1−x}Zr_xO_3$: (a) $x$=0; (b) $x$=0.02; (c) $x$=0.05; (d) $x$=0.08

content. When Zr doping content is 5% (mole fraction), the $CaTi_{1−x}Zr_xO_3$ samples (0≤$x$≤0.08) showed the smallest particle size. The slow rate grain growth for the doped $CaTiO_3$ might be attributed to the presence of interstitial $Zr^{4+}$ ions because the $Zr^{4+}$ ions inhibited the grain growth by providing dissimilar boundaries [25].

TEM images of Zr-doped $CaTiO_3$ are shown in Fig. 2. The images of all samples revealed the uneven size with a few aggregations. The 5%Zr-doped $CaTiO_3$ particles presented the smallest particle size. The average particle size of the 5%Zr-doped $CaTiO_3$ calcined at 850 °C for 3 h was approximately 50 nm. The results were in agreement with the SEM images. Moreover, their particle sizes were larger than their crystallite ones, which were attributed to the reunion of nano-sized crystallite. The elemental composition of the 5%Zr-doped $CaTiO_3$ sample was determined using energy dispersive spectroscopy (EDS) analysis and the result is shown in Fig. 2(e). Zr doping in $CaTiO_3$ was clearly identified from the EDS pattern of 5% Zr-doped $CaTiO_3$. The theoretical mole fraction of the sample was close to the experimental value. Thus, by this co-precipitation reaction it is possible to get desired doping of the metals into $CaTiO_3$ lattice.

The XRD patterns of $CaTi_{1−x}Zr_xO_3$ samples (0≤$x$≤0.08) presented sharp diffraction peaks, and all the diffraction peaks of both as-prepared samples were in a good agreement with the orthorhombic structure of $CaTiO_3$ (JCPDS file No. 42−0423), as shown in

Fig. 3(a). In addition, no impurity peaks were observed in the XRD patterns, which indicated that the as-synthesized samples were of a well-crystallized perovskite phase. It was observed that the peak at $2\theta$=33.1° for $CaTi_{1−x}Zr_xO_3$ samples shifted to lower angles with the increase of Zr content, which showed that the presence of large radius of $Zr^{4+}$ (0.072 nm) might interstitially substitute in $CaTiO_3$ lattice rather substitute for relatively small radius $Ti^{4+}$ (0.065 nm), and this caused lattice distortion in $CaTiO_3$ [23, 26]. When the Zr content was 2%, the peak at $2\theta$=33.1° had a slight shift, indicating that the lattice parameters of $CaTiO_3$ had a minor change due to a small quantity of Zr doping. When the Zr contents were 5% and 8%, respectively, the peak at $2\theta$=33.1° had a large shift and the same level of shift, indicating that Zr could be doped into $CaTiO_3$ up to 5%. Whereas impurity peaks were not observed on the XRD pattern of $CaTi_{0.92}Zr_{0.08}O_3$ sample, the possible reason for this result might be that the XRD is not sensitive enough to detect the minor Zr which is present in other forms. Combined with the XRD patterns of $CaTi_{1−x}Zr_xO_3$ samples, we calculated the average grain sizes of $CaTi_{1−x}Zr_xO_3$ samples according to the Scherrer equation. The average grain sizes for 0, 2%, 5% and 8%Zr-doped $CaTiO_3$ were 33.3, 24.6, 21.5 and 23.4 nm, respectively.

UV−Vis absorption spectral analysis was used to probe the band structure of the as-obtained materials. UV−Vis absorption spectra of $CaTiO_3$ and Zr-doped $CaTiO_3$ are shown in Fig. 4. The modification of $CaTiO_3$
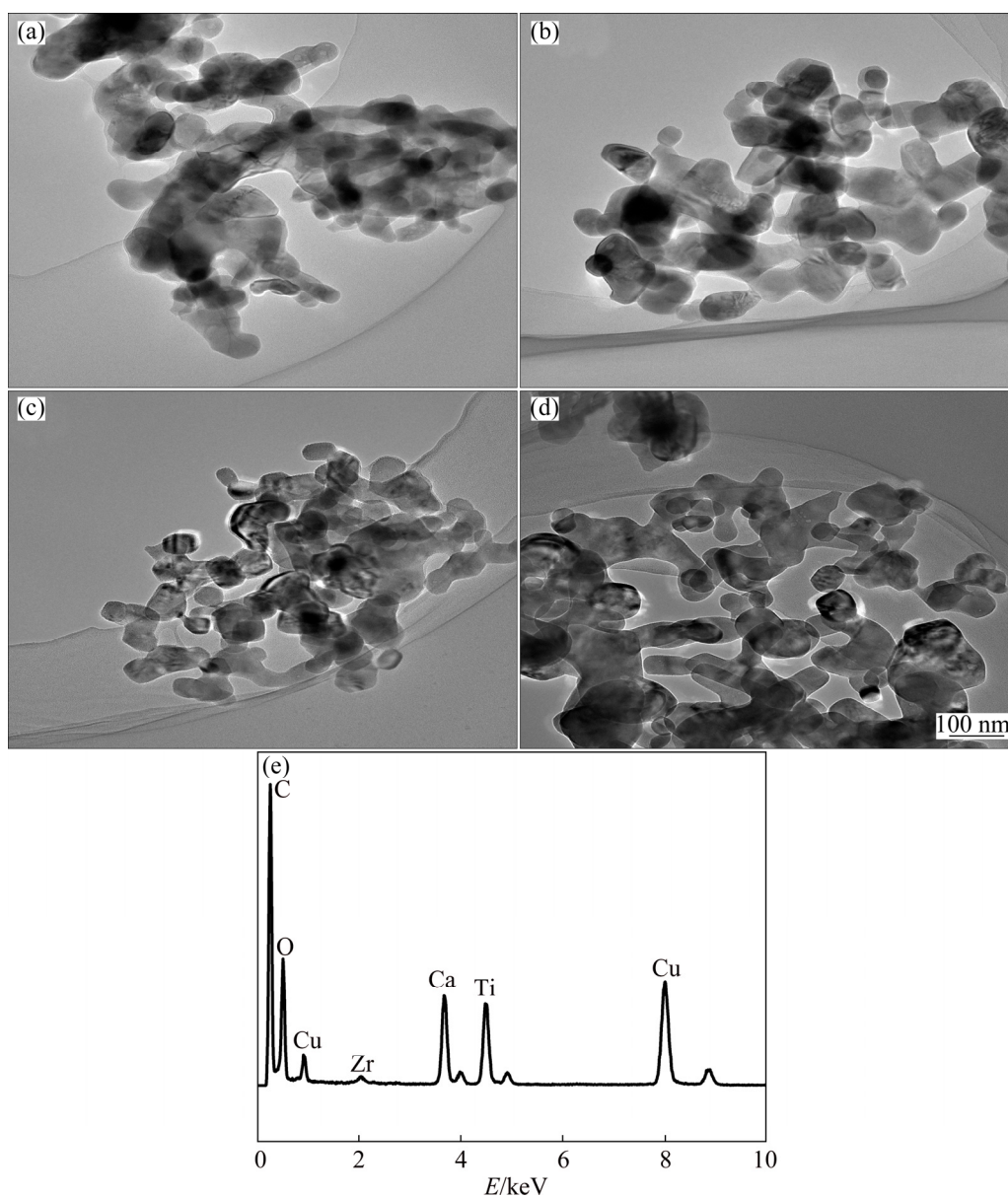
**Fig. 2** TEM images (a−d) and EDS pattern (e) of sintered $CaTi_{1-x}Zr_xO_3$ samples: (a) $x=0$; (b) $x=0.02$; (c) $x=0.05$; (d) $x=0.08$; (e) EDS spectrum of obtained $CaTi_{0.95}Zr_{0.05}O_3$ sample
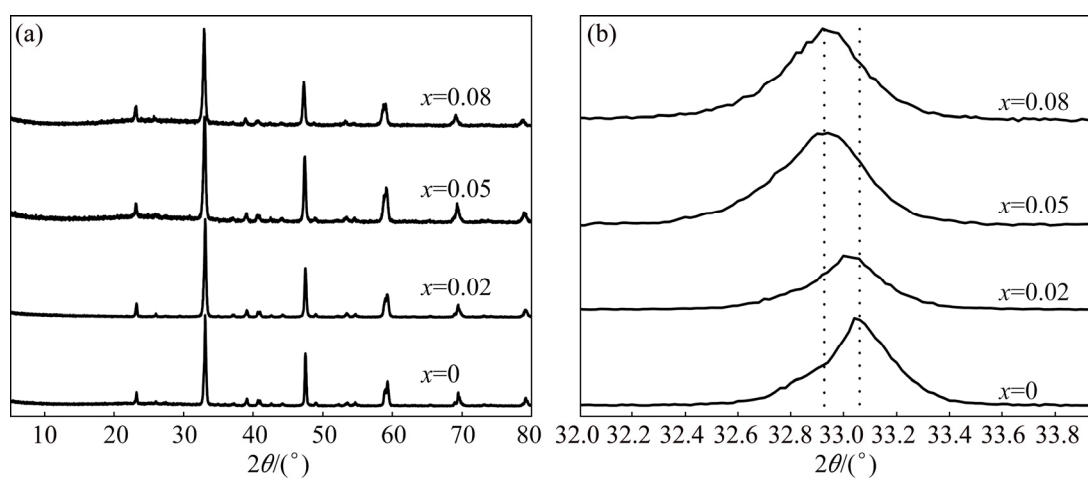


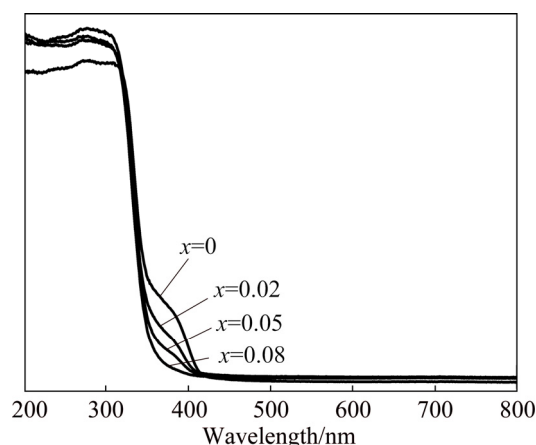**Fig. 3** XRD patterns of $CaTi_{1-x}Zr_xO_3$ (a) and refined peaks near $2\theta$ of 33.1° (b)

**Fig. 4** UV−Vis diffuse reflectance spectra of CaTi$_{1-x}$Zr$_x$O$_3$

with Zr significantly affected the light absorption property of the photocatalysts. The absorbance of Zr-doped CaTiO$_3$ shifted toward shorter wavelength with the increase of Zr content. An optical band gap energy was obtained by plotting $(Ah\upsilon)^2$ versus $h\upsilon$, where $A$ is the absorbance and $h\upsilon$ is photon energy. Extrapolation of the linear portion at $(Ah\upsilon)^2 = 0$ gives the band gap energy. The band gap energies for 0, 2%, 5% and 8%Zr-doped CaTiO$_3$ were 3.47, 3.49, 3.52 and 3.51 eV, respectively. All of the prepared Zr-doped CaTiO$_3$ showed higher band gap energy than CaTiO$_3$. The large band gap was important in preventing the electron−hole recombination and ultimately enhanced the photocatalytic activity [27].

The XPS patterns of Ti, Zr and O elements on the surface of CaTiO$_3$ with different Zr doping contents are shown in Fig. 5. Figure 5(a) showed Ti 2p state, Fig. 5(b) showed Zr 3d state and Fig. 5(c) showed the O 1s state of the perovskite. In Fig. 5(a), the measured binding energy of Ti 2p$_{3/2}$ electrons was within the experimental error, which was consistent with values reported in Ref. [28], showing the presence of Ti$^{4+}$. This meant that the binding energy did not change regardless of the doped Zr content. The Zr 3d XPS patterns of the doped samples are presented in Fig. 5(b). The core level patterns of Zr 3d for the Zr-doped samples showed an increasing intensity along with a slight shift toward lower binding energy with increasing Zr doping up to 5%. This indicated that Zr doping concentration reaches a maximum at 5% Zr doping content. The binding energy of Zr 3d$_{5/2}$ electrons is lower than that of Zr$^{4+}$ ions in ZrO$_2$, 183.5 eV [29]. The observed shift towards lower binding energies can be attributed either to the presence of Zr$^{3+}$ ions or the presence of oxygen vacancies around Zr$^{4+}$ ions. This defect structure may be responsible for higher photocatalytic activity of Zr-doped CaTiO$_3$ in comparison with the undoped CaTiO$_3$ [23]. The photoelectron spectra of O 1s electrons showed the presence of the two components corresponding to the
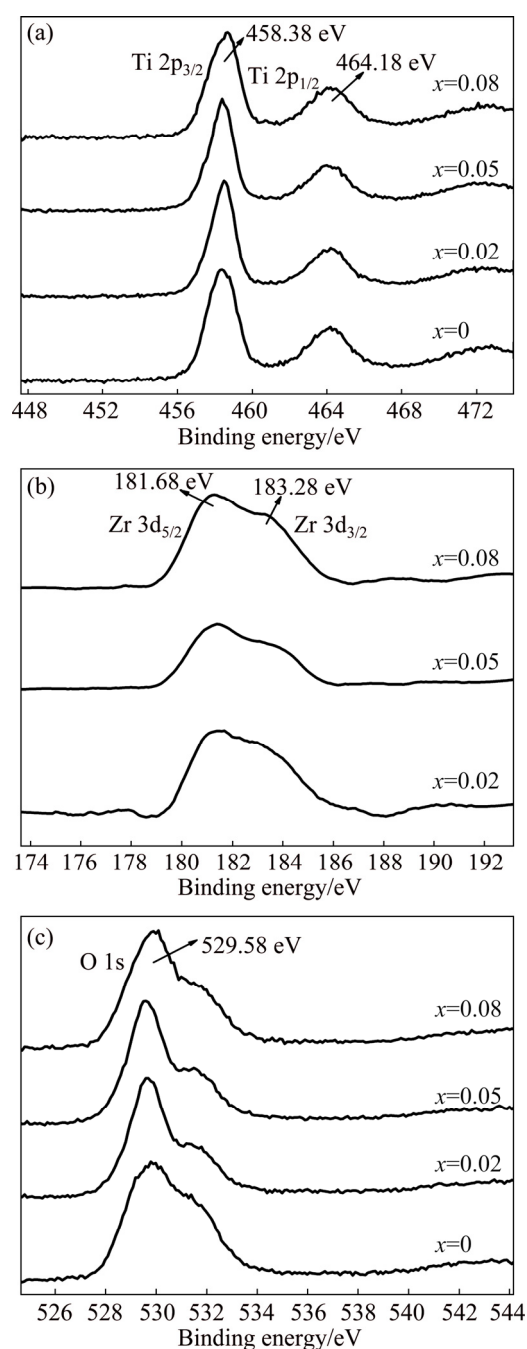


**Fig. 5** XPS patterns of Ti (a), Zr (b) and O (c) elements on surface of CaTi$_{1-x}$Zr$_x$O$_3$

two different chemical states of oxygen, lattice oxygen and adsorbed oxygen with increasing binding energy [29−31]. It could be found that the amount of crystal lattice oxygen decreased with increasing Zr doping content, while the amount of oxygen vacancies increased. The oxygen vacancies are a very active group, which are easily combined with other atoms or groups to become stable. This is responsible for the existence of a certain amount of adsorbed oxygen.

The photogenerated charge separation efficiency could be investigated by the photocurrent spectra under

irradiation of simulated solar light. Figure 6 shows the influence of Zr doping content on the photo-electrochemical activity of CaTiO$_3$ samples. It was shown that the photoelectrochemical activity of all of the Zr-doped CaTiO$_3$ samples was higher than that of the undoped CaTiO$_3$ sample. When the Zr doping content was 5%, the sample showed the highest photo-electrochemical activity, which was 13 times higher than that of the undoped CaTiO$_3$ sample. This clearly indicated that the Zr dopant improved the separation efficiency of photoinduced electrons and holes, and 5%Zr-doped CaTiO$_3$ owned the highest separation efficiency of photoinduced electrons and holes. The introduction of Zr$^{4+}$ into the CaTiO$_3$ lattice could stabilize the current signal. We could suppose that surface oxygen vacancies and defects states by Zr doping could be favorable to capturing the photoinduced electrons during the process of photocatalytic reactions. When the Zr content was 8%, excess amounts of zirconium oxide covering the surface of CaTiO$_3$ would increase the number of recombination centers and resulted in low photocatalytic activity.
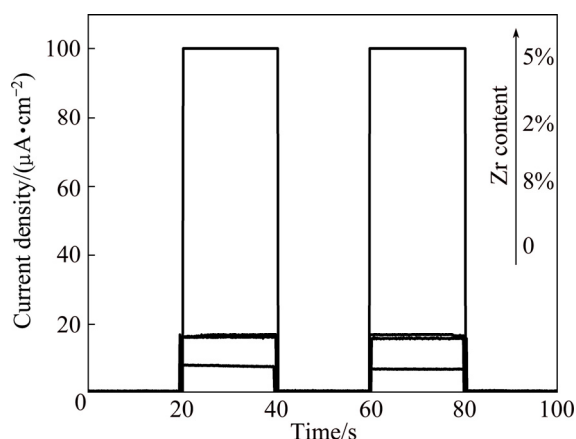


**Fig. 6** Photoresponses of CaTi$_{1−x}$Zr$_x$O$_3$

The photocatalytic activities of different Zr$^{4+}$ doping contents samples calcined at 850 °C for 3 h were evaluated with the degradation rate of methyl orange. Figure 7 shows the degradation rates of various samples after 30 min irradiation. The photocatalytic activity increased with increasing the doping content. When Zr doping content was 5%, the sample showed the highest photocatalytic activity, 91.44% of methyl orange could be degraded after 30 min irradiation. A further increase in doping content reduced the photocatalytic activity. This change is similar to the photogenerated charge separation efficiency change with the increase in Zr content. At the top-right corner of Fig. 7, the kinetics curves of Zr-doped CaTiO$_3$ are shown. As we can see, the photocatalytic reaction processes of all samples were in line with the first order kinetics reaction. The rate

constants increased with increasing doping content. When Zr doping content was 5%, the sample showed the largest rate constant. Combining the UV−Vis diffuse reflectance spectra of different Zr-doped CaTiO$_3$ samples, we speculate that the photogenerated charge separation efficiency is the primary cause that leads to different photocatalytic activities of different Zr doping contents.
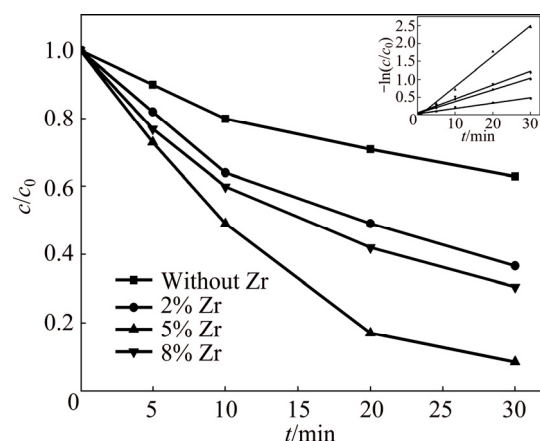


**Fig. 7** Comparison of photocatalytic activity of CaTiO$_3$ with different Zr doping contents

## 4 Conclusions

1) CaTi$_{1−x}$Zr$_x$O$_3$ ($x$=0, 0.02, 0.05, 0.08) perovskites were successfully synthesized by using a mild co-precipitation method.

2) A similar microstructure with fine grain size was observed in all perovskites. The XRD results indicated that Zr$^{4+}$ addition induced a lattice symmetry change. The XPS data confirmed that two types of oxygen existed on the photocatalyst surface, including lattice oxygen and adsorbed oxygen, and more adsorbed oxygen was on the surface of CaTi$_{0.95}$Zr$_{0.05}$O$_3$, which resulted in the formation of more oxygen vacancies.

3) CaTi$_{0.95}$Zr$_{0.05}$O$_3$ showed the highest photo-electrochemical activity. The improved photocatalytic activity was ascribed to the change of the lattice structure, existence of oxygen vacancies and increase of photogenerated charge separation efficiency.

## References

[1]    MILL A, HILL G, BHOPAL S, PARKIN I P, O'NEILL S A. Thick titanium dioxide films for semiconductor photocatalysis [J]. Journal of Photochemistry and Photobiogy A: Chemistry, 2003, 160: 185−194.

[2]    Wu Shui-sheng, JIA Qing-ming, SUN Yan-lin, SHAN Shao-yun, JIANG Li-hong, WANG Ya-ming. Microwave-hydrothermal preparation of flower-like ZnO microstructure and its photocatalytic activity [J]. Transactions of Nonferrous Metals Society of China, 2012, 22: 2465−2470.

[3]    ZHANG Hao, ZONG Rui-long, ZHAO Jin-cai, ZHU Yong-fa. Dramatic visible photocatalytic degradation performances due to synergetic effect of $TiO_2$ with PANI [J]. Environmental Science and Technology, 2008, 42: 3803−3807.

[4]    TONG H, OUYANG S X, BI Y P, UMEZAWA N F, OSHIKIRI M, YE J H. Nano-photocatalytic materials: Possibilities and challenges [J]. Advanced Materials, 2012, 24: 229−251.

[5]    XU Tong-guang, ZHANG Li-wu, CHENG Han-yun, ZHU Yong-fa. Significantly enhanced photocatalytic performance of ZnO via graphene hybridization and the mechanism study [J]. Applied Catalysis B: Environmental, 2011, 101: 382−387.

[6]    LIN J, YU J C. An investigation on photocatalytic activities of mixed $TiO_2$−rare earth oxides for the oxidation of acetone in air [J]. Journal of Photochemistry and Photobiology A: Chemistry, 1998, 116: 63−67.

[7]    KIN C H, QI G S, DAHLBERG K, LI W. Strontium-doped perovskites rival platinum catalysts for treating $NO_x$ in simulated diesel exhaust [J]. Science, 2010, 327: 1624−1627.

[8]    RORIK P M, GRANDE T, EINARSRUD M. One-dimensional nanostructures of ferroelectric perovskites [J]. Advanced Materials, 2011, 23: 4007−4034.

[9]    ZHONG W, VANDERBILT D. Competing structural instabilities in cubic perovskites [J]. Physical Review Letter, 1995, 74: 2587−2590.

[10]   ZHANG Li-li, NIE Yu-lun, HU Chun, QU Jiu-hui. Enhanced fenton degradation of Rhodamine B over nanoscaled Cu-doped $LaTiO_3$ perovskite [J]. Applied Catalysis B, 2012, 125: 418−424.

[11]   BRADHA M, HUSSAIN S, CHAKRABARTY S J, AMARENDRA G, ASHOK A. Total conductivity in Sc-doped $LaTiO_{3+\delta}$ perovskites [J]. Ionics, 2014, 20: 1343−1350.

[12]   ZHANG Cheng-hua, ZHANG Ke, XU Hong-xing, SONG Qi, YANG Yong-tao, YU Ren-hong, XU Dong, CHENG Xiao-nong. Microstructure and electrical properties of sol−gel derived Ni-doped $CaCu_3Ti_4O_{12}$ [J]. Transactions of Nonferrous Metals Society of China, 2012, 22(S1): s127−s132.

[13]   KIM Y, SCHLEGL H, KIM K, IRVINE J T S, KIM J H. X-ray photoelectron spectroscopy of Sm-doped layered perovskite for intermediate temperature-operating solid oxide fuel cell [J]. Applied Surface Science, 2014, 288: 695−701.

[14]   HONG H J, YASHIRO K, HASHIMOTO S, KAWADA T. Conduction properties and ionic transference behavior of $CaTi_{1-x}Sc_xO_{3-\delta}$ ($x$=0.05, 0.1) [J]. ECS Transactions, 2014, 61: 151−157.

[15]   MIZOGUCHI H, UEDA K, ORITA M, MOON S C, KAJIHARA K, HIRANO M, HOSONO H. Decomposition of water by a $CaTiO_3$ photocatalyst under UV light irradiation [J]. Materials Research Bulletin, 2002, 37: 2401−2406.

[16]   ZHANG Hong-jie, CHEN Gang, LI Ying-xuan, TENG Yu-jie. Electronic structure and photocatalytic properties of copper-doped $CaTiO_3$ [J]. International Journal of Hydrogen Energy, 2010, 35: 2713−2716.

[17]   YAN Xin, HUANG Xiao-jun, FANG Ying, MIN Ya-hong, WU Zhen-jun, LI Wen-sheng, YUAN Jian-min. Synthesis of rod-like $CaTiO_3$ with enhanced charge separation efficiency and high photocatalytic activity [J]. International Journal of Electrochemistry Science, 2014, 9: 5155−5163.

[18]   XIAN T, YANG H, HUO Y S. Enhanced photocatalytic activity of $CaTiO_3$−graphene nanocomposites for dye degradation [J]. Physica Scripta, 2014, 89: 115801−115806.

[19]   WU Su-fan, ZHU Yong-fa. Behavior of $CaTiO_3$/Nano-CaO as a $CO_2$ reactive adsorbent [J]. Industrial & Engineering Chemistry Research, 2010, 49: 2701−2706.

[20]   LIU Hai-jin, LIU Guo-guang, ZHOU Qing-xiang. Preparation and characterization of Zr-doped $TiO_2$ nanotube arrays on the titanium sheet and their enhanced photocatalytic activity [J]. Journal of Solid State Chemistry, 2009, 182: 3238−3242.

[21]   CHANG S M, DOONG R A. Characterization of Zr-doped $TiO_2$ nanocrystals prepared by a nonhydrolytic sol−gel method at high temperatures [J]. Journal of Physical Chemistry B, 2006, 110: 20808−20814.

[22]   LUO Qiang, CAI Qi-zhou, LI Xin-wei, PAN Zhen-hua, LI Yu-jie, CHEN Xi-di,YAN Qing-song. Preparation and characterization of $ZrO_2/TiO_2$ composite photocatalytic film by micro-arc oxidation [J]. Transactions of Nonferrous Metals Society of China, 2013, 23(10): 2945−2950.

[23]   LUKÁC J, KLEMENTOVÁ M, BEZDICKA P, BAKARDJIEVA S, ŠUBRT J, SZATMÁRY L, BASTL Z. Influence of Zr as $TiO_2$ doping ion on photocatalytic degradation of 4-chlorophenol [J]. Applied Catalyisis B: Environmental, 2007, 74: 83−91.

[24]   CHANG S M, HOU C Y, LO P H, CHANG C T. Preparation of phosphated Zr-doped $TiO_2$ exhibiting high photocatalytic activity through calcination of ligand-capped nanocrystals [J]. Applied Catalysis B: Environmental, 2009, 90: 233−241.

[25]   BINEESH K V, KIM D K, PARK D W. Synthesis and characterization of zirconium-doped mesoporous nano-crystalline $TiO_2$ [J]. Nanoscale, 2010, 2: 1222−1228.

[26]   GAO B F, LIM T M, SUBAGIO D P, LIM T H. Zr-doped $TiO_2$ for enhanced photocatalytic degradation of bisphenol A [J]. Applied Catalysis A: General, 2010, 375: 107−115.

[27]   KUMARESAN L, MAHALAKSHMI M, PALANICHAMY M, MURUGESAN V. Synthesis, characterization, and photocatalytic activity of $Sr^{2+}$ doped $TiO_2$ nanoplates [J]. Industrial & Engineering Chemistry Research, 2010, 49: 1480−1458.

[28]   JING Li-qiang, SUN Xiao-jun, XIN Bai-fu, WANG Bai-qi, CAI Wei-min, FU Hong-gang. The preparation and characterization of La doped $TiO_2$ nanoparticles and their photocatalytic activity [J]. Journal of Solid State Chemistry, 2004, 177: 3375−3382.

[29]   BASTL Z, SENKEVICH A I, SPIROVOVÁ I, VRTÍLKOVÁ V. Angle-resolved core-level spectroscopy of Zr1Nb alloy oxidation by oxygen, water and hydrogen peroxide [J]. Surface and Interface Analysis, 2002, 34: 477−480.

[30]   WU Hai-hong, DENG Li-xue, WANG Shu-rong, ZHU Bao-liu. The preparation and characterization of La doped $TiO_2$ nanotubes and their photocatalytic activity [J]. Journal of Dispersion Science and Technology, 2010, 31: 1311−1316.

[31]   JING Li-qiang, XU Zi-li, SUN Xiao-jun, SHANG Jing, CAi Wei-min. The surface properties and photocatalytic activites of ZnO ultrafine particles [J]. Applied Surface Science, 2001, 180: 308−314.

# 具有高电荷分离效率和光催化活性的
# 锆掺杂钛酸钙的制备

黄晓俊 [1]，严 欣 [1]，吴海燕 [1]，方 莹 [1]，闵亚红 [1]，李文生 [1]，王双印 [1,2]，吴振军 [1]

1. 湖南大学 化学化工学院，长沙 410082；
2. 湖南大学 化学生物传感与计量学国家重点实验室，长沙 410082

**摘 要**：通过温和共沉淀方法合成一系列锆掺杂的钛酸钙，并在 850 °C 下焙烧 3 h。采用扫描电镜(SEM)、X 射线衍射(XRD)、紫外−可见漫反射光谱(DRS)和 X 射线光电子能谱(XPS)等手段对合成的锆掺杂的钛酸钙进行表征。XRD 结果表明，锆掺杂钛酸钙以单一的钙钛矿相存在；紫外−可见漫反射光谱分析表明，锆掺杂钛酸钙在可见光区的吸收明显增强；XPS 分析显示，在光催化剂表面存在 2 种类型的氧，即晶格氧和吸附氧。此外，对其光催化降解甲基橙的性能以及光电化学性能进行测试。结果表明，5% Zr(摩尔分数)掺杂钛酸钙具有最高光催化活性。晶格结构的改变、氧空穴的存在、光生电荷分离效率的提高都有利于提高锆掺杂的钛酸钙的光催化活性。
**关键词**：钛酸钙；锆；掺杂；共沉淀；光催化；光电化学